Universal dynamics of biological pattern formation in spatio-temporal morphogen variations

Mohit P. Dalwadi[1, 2, *] and Philip Pearce[1, 2, †]

[1] *Department of Mathematics, University College London*
[2] *Institute for the Physics of Living Systems, University College London*

Abstract. In biological pattern-forming systems, generic features have been previously identified that promote robustness with respect to variation between systems in components such as protein production rates and gene-regulatory network architecture. By contrast, less is understood about how individual systems respond to spatio-temporal changes in morphogen concentrations over timescales faster than or similar to cell or tissue growth. Here, we formulate and apply a general theory of biological pattern formation in spatio-temporally varying concentrations of "pre-pattern" morphogens, which determine system parameters. Our analytical results reveal universal dynamical regimes of biological pattern-forming systems, and quantify how the dynamics in each regime depend on the mathematical properties of the relevant gene-regulatory network. By applying our theory, we predict that two paradigmatic pattern-forming systems are robust with respect to spatio-temporal morphogen variations that happen faster than growth timescales. More broadly, we predict that the dynamics of pattern-forming systems with spatio-temporally varying parameters can be classified based on the bifurcations in their governing equations.

INTRODUCTION

In biological pattern formation, concentrations of chemicals termed morphogens are interpreted as signals by cells to make developmental decisions based on their location in a tissue, organ, embryo or population. Such systems have been found to be remarkably robust to a wide range of sources of variation between different cells or tissues in morphogen signals and system components [1, 2]. For example, in recent work, general principles of biological pattern-forming systems have been identified that promote robustness with respect to variations in morphogen and protein production rates [1, 3], in tissue or organism size [4, 5], and in gene-regulatory network architecture [6]. However, less is understood about how such systems respond to spatio-temporal variations in morphogen concentrations within individual cells, populations or tissues over timescales faster than or similar to growth.

Recent experimental and theoretical work has demonstrated how specific gene-regulatory network architectures convert spatio-temporal morphogen signals into a required static or dynamic response [7–12]. This morphogen "pre-pattern" can arise as a necessary part of the developmental process [7, 13, 14]. However, unpredictable morphogen fluctuations in a system may be caused by intrinsic noise [15], growth [16], cell motility or rearrangement [17–20], biochemical reactions [21, 22], or external flows [11, 23–25]. These studies raise the question of how to quantify the robustness of a system's gene-regulatory network output, i.e. emergent spatio-temporal patterning, with respect to variations in its pre-pattern morphogen input.

Here, we introduce a general method to classify and quantify the dynamic response of pattern-forming systems to spatio-temporal variations in their parameters. We use mathematical analysis to show how the dynamics of pattern formation in a system depend on the bifurcations in the underlying equations, which are determined by the system's gene-regulatory network. We apply our framework to classify two paradigmatic pattern-forming systems in terms of their dynamics in variations in pre-pattern morphogens, which affect the kinetics of the gene-regulatory network. Our analysis and simulations suggest that gene-regulatory networks in some biological systems may have been tuned, such that they filter out variations or oscillations in morphogen concentrations that happen much faster than growth, while responding appropriately to physiological morphogen variations.

RESULTS

Canonical pattern-forming systems with spatio-temporal variations

Reaction-diffusion systems, which are thought to underlie various mechanisms of biological pattern formation [7], self organise in space and time via bifurcations in their governing equations [26]. As a reaction-diffusion system undergoes a bifurcation, its dynamics can typically be approximated by a weakly nonlinear canonical equation that depends on the type of bifurcation [27]. Under such an approximation, the effects of spatio-temporal variations in system parameters are captured by corresponding variations in the parameters of the related weakly nonlinear equation. In this paper, we show how these mathematical systems model the dynamics of biological systems with variations in "pre-pattern" morphogens, which determine the kinetic parameters in a gene-regulatory network (Fig. 1).

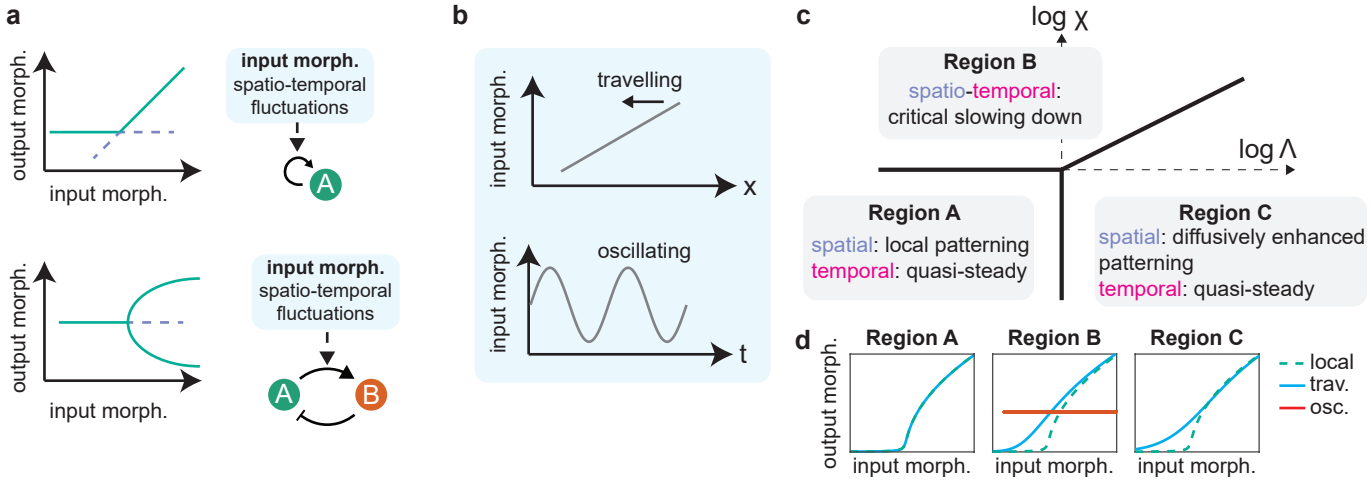

FIG. 1: General asymptotic framework for classifying dynamics of pattern-forming systems. a) Bifurcation diagrams and related minimal gene-regulatory network motifs for two classes of pattern-forming system. Top: autoinduction loops are associated with transcritical bifurcations. Bottom: Activator-inhibitor systems are associated with pitchfork bifurcations. b) Example morphogen concentration input into the asymptotic framework. To make quantitative predictions, we use focus on a travelling gradient (top) and a (spatio-temporal) oscillation (bottom). c) General parameter space that classifies the dynamics in each region, in this case for a travelling gradient causing the switch-off of an imperfect transcritical bifurcation. d) Examples of predicted dynamics in each region of the parameter space, also for an imperfect pitchfork bifurcation. Results were generated by solving Eq. (11) numerically, with $k(x,t)$ specified to be either a travelling gradient or a sinusoidal oscillation, with parameter values corresponding to each region of parameter space. Travelling gradients are indistinguishable from oscillations in Region A and Region C because the system is quasi-steady in those regions. The dashed line shows spatio-temporally local results.

To characterise such systems in general, we analysed the effects of spatio-temporal variations in the parameters of two canonical equations, modified versions of the Fisher-KPP equation and the Ginzburg-Landau equation – these equations represent weakly nonlinear normal forms of transcritical and pitchfork bifurcations, respectively. Each of these bifurcations is closely related to a minimal gene-regulatory motif (Fig. 1a). For a concise summary of our asymptotic results, we focus on two types of spatio-temporal variation in equation parameters: a travelling gradient, and a (spatio-temporal) oscillation. We provide here a sketch of our analysis, focusing on the physiologically relevant cases of switch-on of a transcritical bifurcation and switch-off of a pitchfork bifurcation; the results are summarised in Fig. 1. A more general asymptotic analysis of each system is contained in [28].

Modified Fisher-KPP equation

The weakly nonlinear normal form for (imperfect) transcritical bifurcations relevant to our analysis is a modified Fisher-KPP equation, which in the parameter variations considered here can be written

$$\omega\frac{\partial A}{\partial t} = D\frac{\partial^2 A}{\partial x^2} + a + k(x,t)A - \varepsilon A^2, \qquad (1)$$

where $\varepsilon \ll 1$, and we are typically interested in small values of ω and D. This equation approximates the dynamics of a minimal self-activation motif (Fig. 1a); A is a measure of the concentration of the self-activating morphogen, D represents the strength of diffusion, a represents the strength of base production, k represents the net strength of self-activation (in comparison to decay), and ε represents nonlinear saturation effects. We note that $k = 0$ corresponds to morphogen decay being as fast as morphogen production via self-activation, and is the value of k that causes a transcritical bifurcation in a spatio-temporally uniform system. The parameter ω represents a measure of the frequency of variation in $k(x,t)$.

Travelling gradients: Dynamical regimes

We consider spatio-temporal variations in an input morphogen (Fig. 1a,b), such that the parameter $k(x,t)$ takes the form of a travelling gradient of slope $\eta(t)$,

$$k(x,t) = (x - s(t))\eta(t). \qquad (2)$$

Note that the position of $k = 0$ is described by $x = s(t)$ and moves at speed $\dot{s}(t)$. We transform into the frame around this moving point, scaling $x - s(t)$ with $\varepsilon^{1/2}$ and A with $\varepsilon^{-1/2}$; these scalings are required to balance the reaction terms in Eq. (1) around the bifurcation point. Thus we write,

$$x = s(t) + \sqrt{\varepsilon}X, \quad A = \frac{B}{\sqrt{\varepsilon}}, \qquad (3)$$

to yield

$$\frac{\omega}{\sqrt{\varepsilon}}\frac{\partial B}{\partial t} - \frac{\omega \dot{s}}{\varepsilon}\frac{\partial B}{\partial X} = \frac{D}{\varepsilon^{3/2}}\frac{\partial^2 B}{\partial X^2} + a + X\eta(t)B - B^2. \quad (4)$$

The second term in this equation dominates the first term unless $\dot{s}(t) = O(\sqrt{\varepsilon})$, allowing us to ignore the time derivative. The resulting equation can be simplified and written in terms of only two non-dimensional groupings – to this end, we further rescale using $C = B/\sqrt{a}$ and $Z = \eta X/\sqrt{a}$, which gives

$$0 = \underbrace{\Lambda(t)\frac{\partial^2 C}{\partial Z^2}}_{\text{(i)}} + \underbrace{\chi(t)\frac{\partial C}{\partial Z}}_{\text{(ii)}} + \underbrace{1}_{\text{(iii)}} + \underbrace{ZC}_{\text{(iv)}} - \underbrace{C^2}_{\text{(v)}}, \quad (5)$$

where

$$\Lambda(t) = \frac{\eta^2 D}{(\varepsilon a)^{3/2}}, \quad \chi(t) = \frac{\eta\omega\dot{s}}{\varepsilon a}. \quad (6)$$

These two key groupings can be determined in terms of the parameters in Eq. (1) – if $k(x,t)$ is a travelling wave with constant gradient, both $\dot{s}$ and η are constant and Λ and χ do not depend on time. Broadly, in this system Λ quantifies the importance of diffusion compared to base production and χ quantifies the importance of spatio-temporal changes in the parameters compared to base production.

We have analysed Eq. (5) to characterise all possible dynamical regimes and their dependence on Λ and χ (Fig. 1c). Our analysis shows that three regimes are possible, which we summarise here for a dynamic switch-on, i.e. a function $k(x,t)$ that moves towards the unpatterned region (so that $\dot{s}\eta < 0$ and hence $\chi < 0$):

Region A. Spatially local and quasi-steady patterning. In this case, $\Lambda \ll 1$ and $|\chi| \ll 1$, and terms (iii)-(v) dominate in Eq. (5) – the dynamical position of the bifurcation is $Z = 0$.

Region B. Critical slowing down. In this case $\Lambda^{2/3}/|\chi| \ll 1$ and $|\chi| \gg 1$, and terms (ii)-(v) dominate in Eq. (5) – the dynamical position of the bifurcation is $Z = \sqrt{|\chi|\log|\chi|}$. Saturation, i.e. term (v), can be ignored before switch-on, and base production, i.e. term (iii), can be ignored after switch-on.

Region C. Diffusively enhanced, quasi-steady patterning. In this case $\Lambda \gg 1$ and $\Lambda^{2/3}/|\chi| \gg 1$, and terms (i), (iii)-(v) dominate in Eq. (5) – the dynamical position of the bifurcation is $Z = -\left(\frac{\Lambda}{4}\log^2\Lambda\right)^{1/3}$. Again, saturation can be ignored before switch-on, and base production can be ignored after switch-on.

In each case, the (asymptotic) dynamical position of the bifurcation is located at the position at which the base production term in Eq. (5) is equal to the saturation term (corresponding to $C = 1$).

Oscillations: Critical time period

In finite domains with oscillating parameters, an equilibrium analysis might suggest the repeated emergence and disappearance of a bifurcation at the edge of the domain. However, if the parameters change quickly enough, dynamical effects can cause a delay in the global switch-on or switch-off of such a bifurcation – this suggests the presence of a critical oscillation time period, with implications for robustness. To analyse and quantify this effect, we consider a finite domain $x \in (0,1)$ with Neumann boundary conditions. We impose an oscillatory function $k(x,t)$ and transform into the stationary frame near the edge of the domain at $x = 1$, around the time at which the bifurcation reaches the edge. To balance the reaction terms, we use the scalings

$$x = 1 + \sqrt{\varepsilon}\sigma, \quad t = t^* + \sqrt{\varepsilon}T, \quad A = \frac{B}{\sqrt{\varepsilon}}, \quad (7)$$

where t^* is defined such that $k(1,t^*) = 0$, i.e. t^* is the time at which the bifurcation would be expected to arrive at the boundary of the domain if the problem were quasi-steady. This transforms (1) into

$$\frac{\omega}{\varepsilon}\frac{\partial B}{\partial T} = \frac{D}{\varepsilon^{3/2}}\frac{\partial^2 B}{\partial \sigma^2} + a + \frac{k(1+\sqrt{\varepsilon}\sigma, t^* + \sqrt{\varepsilon}T)}{\sqrt{\varepsilon}}B - B^2. \quad (8)$$

To obtain an analytical result, in the remainder of this subsection we limit ourselves to the case of fast oscillations in long domains before the switch-on of the bifurcation – in this case, spatial and saturation effects are less important and (8) can be approximated by

$$\frac{\omega}{\varepsilon}\frac{\partial B}{\partial T} = a + \hat{k}(T)B, \quad (9)$$

where $\hat{k}(T) = k(1, t^* + \sqrt{\varepsilon}T)/\sqrt{\varepsilon}$, which we leave in its general form at this stage. Eq. (9) can be solved to determine the delayed growth of B on the boundary, which is given by

$$B(0,T) \sim \frac{\varepsilon a}{\omega} e^{\varepsilon \hat{K}(T)/\omega} \int_{-\infty}^{T} e^{-\varepsilon \hat{K}(s)/\omega} \mathrm{d}s, \quad (10)$$

where $\hat{K}(T) = \int_0^T \hat{k}(s)\,\mathrm{d}s = (1/\varepsilon)\int_0^{\sqrt{\varepsilon}T} k(1, t - t^*)\,\mathrm{d}t$. For a specified oscillatory function $k(x,t)$, we calculate the critical oscillation period by identifying whether B reaches a critical value via simple 1D root finding (see Fig. S1).

Modified Ginzburg-Landau equation

The weakly nonlinear normal form for (imperfect, supercritical) pitchfork bifurcations relevant to our analysis is a modified Ginzburg-Landau equation, which in the

parameter variations considered here can be written

$$\omega\frac{\partial A}{\partial t} = D\frac{\partial^2 A}{\partial x^2} + a + k(x,t)A - \varepsilon A^3, \qquad (11)$$

where $\varepsilon \ll 1$, and we are typically interested in small values of ω and D. This equation approximates a minimal activation-inhibition motif (Fig. 1a); A is a measure of the deviation of the concentration of the activating morphogen from the non-patterned state. (More specifically, it represents the amplitude of the envelope of the patterned state, as predicted by the fastest growing mode at the onset of instability.) The parameter D represents the strength of diffusion. The interpretation of the parameter a is less straightforward than in the previous case – in terms of this gene-regulatory motif, a represents a measure of the contribution of any spatially varying base production at the wavenumber of the patterned state. We would typically expect to find $a = 0$ in a system without noise (see below). Similarly to the previous system, the parameter k represents the net strength of self-activation (in comparison to decay), ε represents nonlinear saturation effects, ω represents a measure of the frequency of k variation, and $k = 0$ causes a pitchfork bifurcation in the spatio-temporally uniform system.

Travelling gradients: Dynamical regimes

As before, we consider the parameter $k(x,t)$ to take the form of a travelling gradient (see Eq. 2), and transform into the frame around the moving point $x = s(t)$. In this case, we scale $x - s(t)$ with $\varepsilon^{1/3}$ and A with $\varepsilon^{-1/3}$ to balance the reaction terms in Eq. (11) around the bifurcation point. Incorporating an additional scaling concurrently, in order to write the resulting equation in terms of two non-dimensional groupings, we introduce the scaled variables

$$Z = \frac{\eta(x - s(t))}{(\varepsilon a^2)^{1/3}}, \quad A = \left(\frac{a}{\varepsilon}\right)^{1/3} C. \qquad (12)$$

Similarly to the transcritical case, this scaling results in the leading-order governing equation:

$$0 = \Lambda(t)\frac{\partial^2 C}{\partial Z^2} + \chi(t)\frac{\partial C}{\partial Z} + 1 + ZC - C^3, \qquad (13)$$

where now

$$\Lambda(t) = \frac{\eta^2 D}{\varepsilon a^2}, \quad \chi(t) = \frac{\eta\omega\dot{s}}{(\varepsilon a^2)^{2/3}}. \qquad (14)$$

By analysing Eq. (13), we find the same three regimes as for the transcritical case (Fig. 1c), but with differences in the dynamical positions of the bifurcation. In contrast to the transcritical case, we summarise the results here for dynamic switch-off, i.e. a function $k(x,t)$ that moves towards the patterned region (so that $\dot{s}\eta > 0$ and hence $\chi > 0$):

Region A. Spatially local and quasi-steady patterning. In this case, $\Lambda \ll 1$ and $\chi \ll 1$, and the dynamical position of the bifurcation is $Z = 0$.

Region B. Critical slowing down. In this case $\Lambda^{2/3}/\chi \ll 1$ and $\chi \gg 1$, and the dynamical position of the bifurcation is $Z = -\sqrt{\frac{\chi}{2}\log\chi}$.

Region C. Diffusively enhanced, quasi-steady patterning. In this case $\Lambda \gg 1$ and $\Lambda^{2/3}/\chi \gg 1$, and the dynamical position of the bifurcation is $Z = -\left(\frac{\Lambda}{16}\log^2\Lambda\right)^{1/3}$.

In this case, the dominating terms in each region are similar to those in the transcritical case.

Special case: Perfect bifurcations

As we will see later, in typical applications it is of interest to consider the case of a perfect bifurcation, where $a = 0$. This is a singular limit that involves a fundamental change in the far-field behaviour of the local system. The key dimensionless parameter grouping here is

$$\Gamma(t) := \frac{\chi(t)}{[\Lambda(t)]^{2/3}} = \frac{\omega\dot{s}}{(\eta D^2)^{1/3}}, \qquad (15)$$

which quantifies the importance of spatio-temporal changes in the parameters compared to diffusion. We focus here on the dynamical switch-off of a pattern which corresponds to $\Gamma > 0$ (from $\eta\dot{s} > 0$). Using the scaled quantities

$$\xi = \left(\frac{\eta}{D}\right)^{1/3}(x - s(t)), \quad Y = \frac{\varepsilon^{1/2}}{D^{1/6}|\eta|^{1/3}}A, \qquad (16)$$

the leading-order version of Eq. (11) with $a = 0$ becomes

$$0 = \frac{\partial^2 Y}{\partial \xi^2} + \Gamma(t)\frac{\partial Y}{\partial \xi} + \xi Y - Y^3. \qquad (17)$$

By analysing Eq. (17), we find that in this case only two of the previously identified regimes can be exhibited:

Region B. Critical slowing down. In this case, $\Gamma \gg 1$.

Region C. Diffusively enhanced, quasi-steady patterning. In this case $\Gamma \ll 1$.

In the case of perfect bifurcations, natural definitions of the location of the dynamic bifurcation typically depend on the initial conditions [29]. In practice, in the applications considered here, emergent patterns are highly oscillatory; therefore, for consistency we use the wavelength of the fastest growing mode at the onset of the instability to define the critical size of Y at switch-off (Fig. S1).

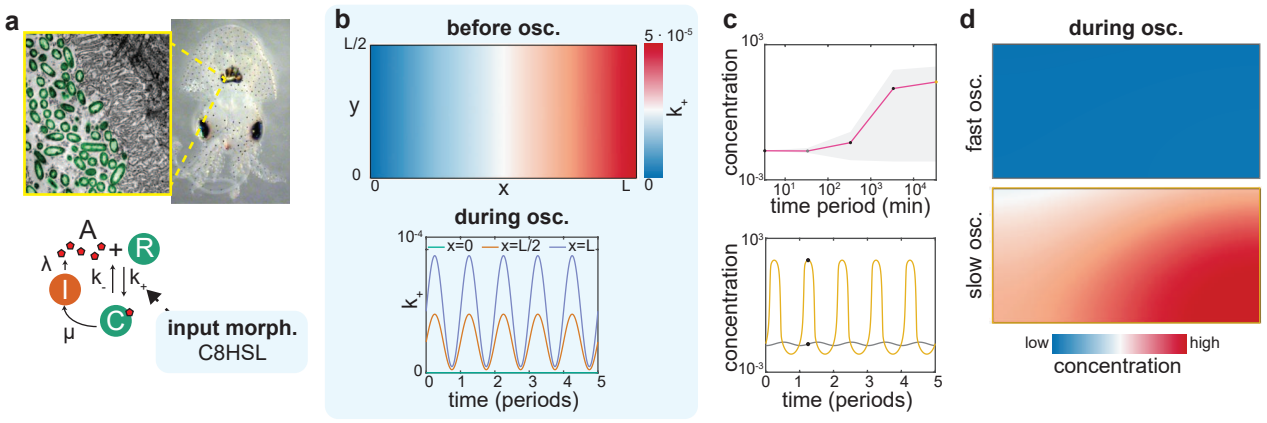

FIG. 2: Effect of spatio-temporal morphogen variations on bacterial quorum sensing in a small biofilm or cell population. a) We model quorum sensing in *V. fischeri*, which causes bioluminescence in the Hawaaian bobtail squid (top; images adapted from [30], with permission). We model the LuxR system, in which an autoinducer, 3OC6HSL, promotes its own synthesis by binding with a protein, LuxR, to form a transcription factor (bottom). The binding parameter k_+ is modulated by competitive binding with a second autoinducer, C8HSL. b) The parameter k_+ (units: $\mathrm{nM}^{-1}\mathrm{s}^{-1}$) at $t = 0$ (top) and throughout the spatio-temporal oscillations (bottom). c) Top: Effect of the time period T of the spatio-temporal oscillations in C8HSL on the mean 3OC6HSL concentration (line), and the range of 3OC6HSL concentration (grey area) during the oscillations. Bottom: Oscillations in 3OC6HSL concentration, for fast ($T \approx 30$ min) and slow ($T \approx 3 \cdot 10^4$ min) oscillations in C8HSL. d) For oscillations that are filtered out, the system remains at low 3OC6HSL concentration (top). For oscillations that are not filtered out, the cell population fills with 3OC6HSL during th oscillation (bottom). Images correspond to the black dots in the bottom graph of panel c. Concentrations in the figure are scaled by the quorum sensing activation threshold of 5 nM [11].

Oscillations: Critical time period

We again consider an oscillatory function $k(x,t)$ and transform into the stationary frame near the edge of the domain $x = 1$, around the time at which the bifurcation reaches the edge. In this case we assume $a = 0$. To balance the reaction terms, we use the scalings

$$x = 1 + \varepsilon^{1/3}\sigma, \quad t = t^* + \varepsilon^{1/3}T, \quad A = \frac{B}{\varepsilon^{1/3}}, \tag{18}$$

where $k(1, t^*) = 0$. This transforms (11) into

$$\frac{\omega}{\varepsilon^{2/3}}\frac{\partial B}{\partial T} = \frac{D}{\varepsilon}\frac{\partial^2 B}{\partial \sigma^2} + \frac{k(1+\varepsilon^{1/3}\sigma, t^* + \varepsilon^{1/3}T)}{\varepsilon^{1/3}}B - B^3. \tag{19}$$

In the case of fast oscillations in long domains before the switch-off of the bifurcation, Eq. (19) can be approximated by

$$\frac{\omega}{\varepsilon^{2/3}}\frac{\partial B}{\partial T} = \hat{k}(T)B - B^3, \tag{20}$$

where $\hat{k}(T) = k(1, t^* + \varepsilon^{1/3}T)/\varepsilon^{1/3}$, which can be solved to give

$$B(0,T) \sim \frac{\omega^{1/2}}{\varepsilon^{1/3}} \frac{e^{\varepsilon^{2/3}F(T)/\omega}}{\sqrt{2\int_{-\infty}^{T} e^{2\varepsilon^{2/3}F(s)/\omega}\,\mathrm{d}s}}, \tag{21}$$

where $F(T) = \int_0^T \hat{k}(s)\,\mathrm{d}s = (1/\varepsilon^{2/3})\int_0^{\varepsilon^{1/3}T} k(1, t - t^*)\,\mathrm{d}t$. For a specified oscillatory function $k(x,t)$, we calculate the critical oscillation period via 1D root finding, as before (Fig. S1).

Biological pattern-forming systems with spatio-temporal variations

We now explore the implications of our analytical results to biological pattern-forming systems with variations in "pre-pattern" morphogens. We analyze and simulate two pattern-forming systems in which an input morphogen concentration determines the kinetic parameters in the gene-regulatory network: bacterial quorum sensing, in which changes in the kinetic parameters cause a transcritical bifurcation, and a model for digit formation via Turing patterns, in which changes in the kinetic parameters cause a pitchfork bifurcation.

Transcritical system: Bacterial quorum sensing

Model. We consider the LuxR bacterial quorum sensing system in *Vibrio fischeri*, which causes bioluminescence in the Hawaaian bobtail squid [31]. We model a population, biofilm or cell layer of height H and length L, and consider the influence of two autoinducers, 3OC6HSL and C8HSL, with cross-talk between them [32]. We model this basic mechanism of autoinducer crosstalk for simplicity; more complicated crosstalk mechanisms have been found (e.g. [33]). We model the

concentration A of one of the autoinducers, 3OC6HSL, which is part of a positive feedback loop: it forms a complex C with a cognate protein LuxR (R) that activates the expression of LuxI (I), a synthase that catalyses the expression of 3OC6HSL (Fig. 2a). The system is described by the equations

$$\frac{\partial A}{\partial t} = \nabla \cdot (D\nabla A) + \rho f_A(A, I, R, C; x, t) - \kappa A, \tag{22}$$

$$\frac{\partial I}{\partial t} = f_I(I, C),\ \frac{\partial R}{\partial t} = f_R(A, R, C),\ \frac{\partial C}{\partial t} = f_C(A, R, C). \tag{23}$$

Here, D is the diffusivity of 3OC6HSL, ρ is the volume fraction of cells-to-total-volume, κ is the decay rate of 3OC6HSL, and the reaction terms inside each bacterium are defined as the following:

$$f_A(A, I, R, C) = a + \lambda I + k_- C - k_+(x, t) AR, \tag{24a}$$

$$f_I(I, C) = \mu C - \alpha I, \tag{24b}$$

$$f_R(A, R, C) = r - \beta R + k_- C - k_+(x, t) AR, \tag{24c}$$

$$f_C(A, R, C) = k_+(x, t) AR - k_- C - \gamma C, \tag{24d}$$

where the kinetic parameters are described in the Supplemental Material. We consider the effects of environmental fluctuations in, for example, external fluid flow, temperature, light, or antibiotic treatment. Such changes can affect gene expression profiles, community composition [34–36], or, as in the case of fluid flow, act directly on autoinducer concentrations [11] (with effects depending on each autoinducer's effective diffusion coefficient, as determined by interactions with extracellular matrix proteins [37]). In each case, the relative concentrations of the autoinducers would be expected to vary. Here we aim to capture such differential variations in a simple way by modelling only changes in C8HSL concentration; we assume that they predominantly affect the binding of 3OC6HSL to LuxR, and therefore let $k_+(x, t)$ vary in space and time as follows:

$$k_+(x, t) = k_+^R f(x, t), \tag{25}$$

where k_+^R is a typical value of the binding coefficient. For simplicity, we investigate two different types of spatio-temporal variation: one with the form of a linear gradient in space travelling with constant speed

$$f(x, t) = x/L - t/T, \tag{26}$$

and one with a linear gradient in space and a sinusoidal oscillation in time

$$f(x, t) = (x/L)\,(1 + K \sin(2\pi t/T)), \tag{27}$$

where K quantifies the relative magnitude of the oscillation (see Supplemental Material). This model could easily be extended to account explicitly for fluctuations in external flow or cell density [11]. We note that our model assumes that the C8HSL-LuxR complex does not promote the expression of LuxR, in line with experimental findings [32].

Analysis. We show in the Supplemental Material that with a travelling gradient in the kinetic parameter (Eq. 26), this system reduces to Eq. (5), with $\Lambda(t)$ and $\chi(t)$ written in terms of the kinetic parameters (Eq. S29). For physiologically relevant values of the parameters in a small bacterial population or biofilm (Table S1), with the timescale of variation T corresponding to a growth timescale, our analysis predicts that the system sits in Regime C of parameter space (diffusively enhanced patterning; see Fig. 1c). Specifically, because our analysis outputs the dynamical location of the bifurcation, we predict that diffusive enhancement causes the switched-on region to be larger than the size of the population (Table S1). Therefore, any local switch on in quorum sensing caused by changes over a growth timescale would be expected to cause the entire population to switch on.

Interestingly, by varying the timescale T in Eq. (26), we find that if C8HSL concentration changes faster than a critical timescale of around 30 minutes (Table S1), the system transitions to Region B (critical slowing down) of parameter space. To investigate the implications of this critical timescale, we analysed the system dynamics with oscillatory kinetic parameters by applying Eq. (10) to a long, thin cell layer (Table S1), for which this thin-film result is expected to be valid. With oscillations of the form Eq. (27), we found that if T is shorter than around 3-10 hours (Fig. S1), the oscillations occur fast enough to cause the system to remain stuck in the switched-off state, because of the critical slowing down in the system. Therefore, we expect changes in C8HSL concentration to be ignored if they occur much faster than a growth timescale.

Simulations. To confirm our findings, we performed simulations in the finite-element computational software COMSOL Multiphysics of a small biofilm or cell population in two dimensions, with the switched-off state as the initial condition. We imposed oscillations in k_+ of the form Eq. (27), for physiological values of the parameters (Fig. 2b, Table S1; see Supplemental Material for further details). Our simulations demonstrate that if oscillations happen over timescales much faster than growth, the system remains stuck in the switched-off state, and that the system responds to slower changes in k_+ (Fig. 2c), in qualitative agreement with our asymptotic results. We also simulated long, thin cell layers [23] for which the thin-film result Eq. (21) is expected to be valid, and found quantitative agreement in the critical oscillation time period (Fig. S1). Furthermore, our simulations confirm that when the bifurcation is switched on, the domain fills with autoinducers because of the diffusive enhancement in the system (Fig. 2d).

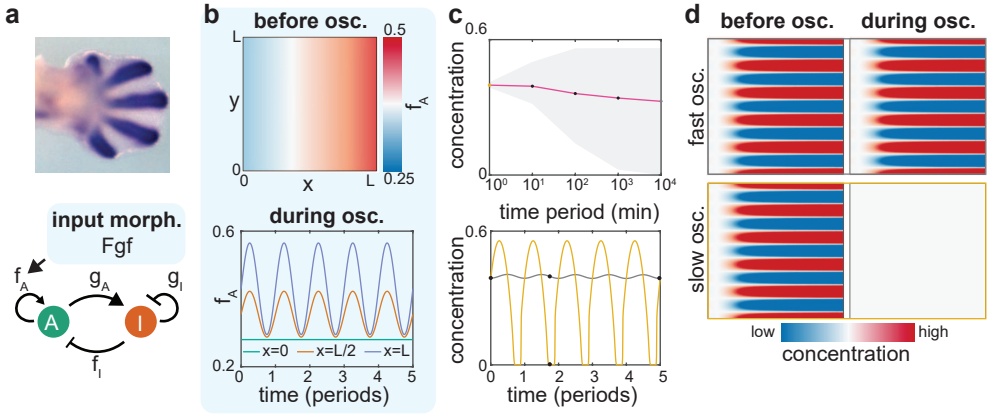

FIG. 3: Effect of spatio-temporal morphogen variations on Turing patterns. a) We model Turing patterns during digit formation (top; image reproduced from [14] with permission). The system's pattern can be represented as an activator-inhibitor system, with the self-activation parameter f_A modulated by a morphogen called Fgf (bottom). b) The parameter f_A (units: min^{-1}) at $t = 0$ (top) and throughout the spatio-temporal oscillations (bottom). c) Top: Effect of time period T of spatio-temporal oscillations in Fgf on the mean concentration of the activator morphogen (line), and the range of concentration (grey area) during the oscillations. Bottom: Oscillations in the activator morphogen concentration for fast ($T = 1$ min) and slow ($T = 10^4$ min) oscillations in Fgf. d) For oscillations that are filtered out, patterning remains the same (top). For oscillations that are not filtered out, patterning completely disappears (bottom). Images correspond to the black dots in the bottom graph of panel c. Concentrations in the figure are non-dimensional and represent deviation from a base state at $x = 0$ [16].

Pitchfork system: Turing patterns during development

Model. We consider the Turing pattern that is thought to promote digit formation [14]. We model a limb of height H and length L with an activator of concentration A and an inhibitor of concentration I, and consider the effect of a morphogen called fibroblast growth factor (Fgf), which controls the self-activation of the activator (Fig 3a). The system is described by the equations

$$\frac{\partial A}{\partial t} = D_A \frac{\partial^2 A}{\partial x^2} + f_A(x,t)A - f_I I - f_c A^3, \tag{28}$$

$$\frac{\partial I}{\partial t} = D_I \frac{\partial^2 I}{\partial x^2} + g_A A - g_I I, \tag{29}$$

where D_A and D_I are diffusion coefficients and f_A, f_I, g_A and g_I are kinetic parameters. To simulate variations in the concentration of the Fgf morphogen [14], we let $f_A(x,t)$ vary in space and time by setting

$$f_A(x,t) = f_A^b + k_A f(x,t), \tag{30}$$

where f_A^b is the base self-activation, and k_A is a typical increase in the self-activation. As before, we investigate two different types of spatio-temporal variation: one with the form of a linear gradient in space travelling with constant speed

$$f(x,t) = x/L - t/T, \tag{31}$$

and one with a linear gradient in space and a sinusoidal oscillation in time

$$f(x,t) = (x/L)\left(1 + K \sin\left(2\pi t/T\right)\right), \tag{32}$$

where K quantifies the relative magnitude of the oscillation (see Supplemental Material). For simplicity, we fix the other parameters, although more detailed models could also involve oscillations in those parameters, or could consider Turing patterns formed by more complicated gene-regulatory networks [14, 16].

Analysis. We show in the Supplemental Material that with a travelling gradient in the kinetic parameter (Eq. 31), this system reduces to Eq. (17), with $\Gamma(t)$ written in terms of the kinetic parameters (Eq. S53). For physiologically relevant values of the parameters (Table S2), with the timescale of variation T corresponding to a growth timescale, our analysis predicts that the system sits in Region C of parameter space (diffusively enhanced patterning; see Fig. 1c). Similarly to the transcritical system, we are able to predict the size of diffusive enhancement in this system; in this case, we find the enhancement to the switched-on region to be less than 10% of the size of the domain (Table S2). Therefore, we expect patterns generated by variations in Fgf concentration over a growth timescale to be relatively localised to the region in which Fgf concentration is above its critical value for patterning.

In contrast to the transcritical system, here we find a critical timescale T of approximately 5 hours for a travelling gradient (Table S2) in Eq. (26), below which the system transitions to Region B of parameter space (critical slowing down). By applying Eq. (21) with oscillations of the form Eq. (32), we find a critical oscillation timescale of around 10 hours (Fig. S1). Therefore, we expect changes in Fgf concentration to be ignored by the

system if they occur much faster than a growth timescale.

Simulations. To confirm our findings, we performed simulations of the system in two dimensions for physiological values of the parameters (Table S2). In this case, we used as initial condition the patterned state with horizontal stripes, which corresponds to the physiologically relevant switched-on state [14] (Fig. 3b; see Supplemental Material for further details). Our simulations again confirmed the analytical results qualitatively and quantitatively (Fig. 3c, Fig. S1). In particular, our results show that the system ignores oscillations in f_A that occur much faster than growth, even if they are large enough such that an equilibrium analysis would predict the pattern to completely disappear (Fig. 3c).

DISCUSSION

Universal dynamics of pattern-forming systems. This study characterises the effects of spatio-temporally varying parameters on pattern-forming systems. We have demonstrated that such systems exhibit universal dynamics that are determined by the underlying bifurcations in their governing equations. Systems that undergo transcritical and pitchfork bifurcations are described by modified versions of the Fisher–KPP (Eq. 1) and Ginzburg–Landau (Eq. 11) equations, respectively. Through analysis of these canonical equations, we have identified universal parameter regimes: the emergent system dynamics are determined in time and space by the regime in which the parameters lie (Fig. 1b-d). We have quantified how, in each regime, a dynamic bifurcation is determined either locally or non-locally by the system parameters in space and time (Fig. 1c,d) – broadly, spatial non-locality is associated with diffusion and temporal non-locality is associated with dynamic variations in the parameters. A striking example of spatio-temporal non-locality is the "critical slowing down" regime, in which dynamics are slowed by the bifurcation and the system may become stuck in the "off" or "on" state, despite large variations in its parameters (Fig. 1d). These results complement recent work on pattern formation in various systems of equations with spatio-temporally varying parameters (e.g. [10, 38–45]) and on the effect of critical slowing down in a range of contexts [46, 47]. Overall, our analytical results improve our fundamental understanding of how the mathematical properties of a pattern-forming system's underlying equations determine the system's emergent dynamics.

Robustness of biological pattern-forming systems. We have demonstrated the biological implications of our analysis by applying our method to two pattern-forming systems with spatio-temporally varying morphogens: bacterial quorum sensing with variations in a cross-talking autoinducer, and digit formation with variations in fibroblast growth factor. We have shown that both systems are subject to the universal regimes that we have identified, by reducing the governing equations to their corresponding weakly nonlinear canonical forms. Interestingly, our analysis predicts that in oscillatory morphogen variations in which the kinetic parameters pass through their bifurcation values and then return to their original values, both biological systems change dynamical regime depending on the magnitude and time period of the oscillations. For fast enough morphogen oscillations, the systems remain in the "critical slowing down" regime of parameter space, and no dynamic bifurcation occurs. However, in each system, if morphogen oscillations are slow enough, the system leaves this region of parameter space and a dynamical bifurcation occurs. These results have significant implications for understanding and quantifying the robustness of pattern-forming systems to changes in morphogen concentrations. For example, we predict that both systems filter out changes that occur much faster than growth, in line with experimental evidence that suggests physiologically relevant changes to patterning in each system happen over growth timescales [14, 16, 48].

Furthermore, our analyses and simulations suggest that the effects of diffusion in each system are quantitatively different. In the bacterial quorum sensing system, we predict significant levels of "diffusively enhanced patterning" – the autoinducers flood the entire population or biofilm after a bifurcation occurs. This would be expected to benefit the population by ensuring all cells commit together to a multicellular program of gene expression [11]. By contrast, diffusive enhancement to patterning is much weaker in the Turing system, so that patterning would be expected to be controlled relatively locally by the concentration of the input morphogen Fgf. This prediction is in line with recent analyses of Turing systems in steady "pre-pattern" morphogen gradients, in which patterning was found to be controlled relatively locally in space [10].

In modelling the biological systems in this paper we have performed significant simplifications to extract general results, and to improve the clarity of our analysis and exposition. In particular, for simplicity we have specified morphogen variations to be linear in space and either travelling at constant speed or sinusoidally oscillating in time, although our results hold more generally [28]. We have not modelled the effect of white noise, which we expect to have non-trivial effects that are not captured by our analysis [49, 50]. Furthermore, our models are effective macroscopic representations of microscopic processes, and the process of coarse-graining the microscopic dynamics to obtain effective macroscopic dynamics is often not trivial [51].

General applications to pattern-forming systems. In principle, any pattern-forming system that undergoes a transcritical or pitchfork bifurcation can be analysed using our asymptotic framework and plotted

on the parameter space that our analysis has produced (Fig. 1c), to classify and quantify its dynamics in spatio-temporal morphogen variations. We expect that our results can also be extended to wider classes of systems, such as those with Hopf bifurcations in their underlying governing equations. Our general framework to classify the dynamics of gene-regulatory network architectures via their low-dimensional mathematical structure (i.e. bifurcations) complements recent work on dimensionality reduction of systems without spatio-temporal heterogeneity [52–54] and systems transitioning from a dynamic to a static regime [21].

Conclusion. To conclude, we have presented a general framework that classifies and quantifies the dynamic response of pattern-forming systems to spatio-temporal variations in their parameters. We have applied our framework to simple models of two biological pattern-forming systems, each with variations in a pre-pattern morphogen that affects kinetic parameters: bacterial quorum sensing, and digit formation via Turing patterns. Our theory predicts that both systems filter out spatio-temporal morphogen variations that occur much faster than growth. We demonstrate that the type of bifurcation in the system, which is determined by the gene-regulatory network, controls patterning dynamics and structure. Predictions such as these are testable in newly developed systems that allow spatio-temporal control over gene-expression and the external environment, such as synthetic model organisms [55], organoids [56] and microfluidic devices [23]. Owing to the generality of the canonical equations that we have analysed, our theoretical framework is extendable to a wide class of pattern-forming systems.

Acknowledgements. MPD is supported by the UK Engineering and Physical Sciences Research Council [Grant No. EP/W032317/1]. We acknowledge Zena Hadjivasiliou and Jake Cornwall Scoones for helpful discussions, and Eric Stabb for assistance in preparing Fig. 2a.

* m.dalwadi@ucl.ac.uk; equal contribution
† philip.pearce@ucl.ac.uk; equal contribution

[1] Alon, U. *An Introduction to Systems Biology* (Chapman and Hall/CRC, Second edition. — Boca Raton, Fla. : CRC Press, [2019], 2019).
[2] Vittadello, S. T., Leyshon, T., Schnoerr, D. & Stumpf, M. P. H. Turing pattern design principles and their robustness. *Philosophical Transactions of the Royal Society A: Mathematical, Physical and Engineering Sciences* **379** (2021).
[3] Eldar, A. *et al.* Robustness of the BMP morphogen gradient in Drosophila embryonic patterning. *Nature* **419**, 304–308 (2002).
[4] Wartlick, O. *et al.* Dynamics of Dpp Signaling and Proliferation Control. *Science* **331**, 1154–1159 (2011).
[5] Mateus, R. *et al.* BMP Signaling Gradient Scaling in the Zebrafish Pectoral Fin. *Cell Reports* **30**, 4292–4302 (2020).
[6] Scholes, N. S., Schnoerr, D., Isalan, M. & Stumpf, M. P. A Comprehensive Network Atlas Reveals That Turing Patterns Are Common but Not Robust. *Cell Systems* **9**, 243–257 (2019).
[7] Green, J. B. A. & Sharpe, J. Positional information and reaction-diffusion: two big ideas in developmental biology combine. *Development* **142**, 1203–1211 (2015).
[8] Jutras-Dubé, L., El-Sherif, E. & François, P. Geometric models for robust encoding of dynamical information into embryonic patterns. *eLife* **9**, 1–36 (2020).
[9] Cornwall Scoones, J. & Hiscock, T. W. A dot-stripe Turing model of joint patterning in the tetrapod limb. *Development* **147** (2020).
[10] Krause, A. L., Klika, V., Woolley, T. E. & Gaffney, E. A. From one pattern into another: Analysis of Turing patterns in heterogeneous domains via WKBJ. *Journal of the Royal Society Interface* **17** (2020).
[11] Dalwadi, M. P. & Pearce, P. Emergent robustness of bacterial quorum sensing in fluid flow. *Proceedings of the National Academy of Sciences of the United States of America* **118**, e2022312118 (2021).
[12] Krause, A. L., Gaffney, E. A., Maini, P. K. & Klika, V. Modern perspectives on near-equilibrium analysis of Turing systems. *Philosophical Transactions of the Royal Society A: Mathematical, Physical and Engineering Sciences* **379** (2021).
[13] Turing, A. M. The chemical basis of morphogenesis. *Philosophical Transactions of the Royal Society of London. Series B, Biological Sciences* **237**, 37–72 (1952).
[14] Sheth, R. *et al.* Hox Genes Regulate Digit Patterning by Controlling the Wavelength of a Turing-Type Mechanism. *Science* **338**, 1476–1480 (2012).
[15] Paulsson, J. Summing up the noise in gene networks. *Nature* **427**, 415–418 (2004).
[16] Raspopovic, J., Marcon, L., Russo, L. & Sharpe, J. Digit patterning is controlled by a Bmp-Sox9-Wnt Turing network modulated by morphogen gradients. *Science* **345**, 566–570 (2014).
[17] Ward, J. P. *et al.* Early development and quorum sensing in bacterial biofilms. *Journal of Mathematical Biology* **47**, 23–55 (2003).
[18] Daniels, R., Vanderleyden, J. & Michiels, J. Quorum sensing and swarming migration in bacteria. *FEMS Microbiology Reviews* **28**, 261–289 (2004).
[19] Bhattacharyya, S. & Yeomans, J. M. Coupling Turing stripes to active flows. *Soft Matter* **17**, 10716–10722 (2021).
[20] Fulton, T. *et al.* Cell Rearrangement Generates Pattern Emergence as a Function of Temporal Morphogen Exposure. *bioRxiv* (2022).
[21] Wigbers, M. C. *et al.* A hierarchy of protein patterns robustly decodes cell shape information. *Nature Physics* **17**, 578–584 (2021).
[22] Patel, K., Rodriguez, C., Stabb, E. V. & Hagen, S. J. Spatially propagating activation of quorum sensing in Vibrio fischeri and the transition to low population density. *Physical Review E* **101**, 062421 (2020).
[23] Kim, M. K., Ingremeau, F., Zhao, A., Bassler, B. L. & Stone, H. A. Local and global consequences of flow on bacterial quorum sensing. *Nature Microbiology* **1**, 15005 (2016).

[24] Mukherjee, S. & Bassler, B. L. Bacterial quorum sensing in complex and dynamically changing environments. *Nature Reviews Microbiology* **17**, 371–382 (2019).

[25] Pearce, P. *et al.* Flow-Induced Symmetry Breaking in Growing Bacterial Biofilms. *Physical Review Letters* **123**, 258101 (2019).

[26] Brauns, F., Halatek, J. & Frey, E. Phase-Space Geometry of Mass-Conserving Reaction-Diffusion Dynamics. *Physical Review X* **10**, 041036 (2020).

[27] Strogatz, S. H. *Nonlinear Dynamics and Chaos* (CRC Press, 2015).

[28] Dalwadi, M. & Pearce, P. Dynamic bifurcations in spatio-temporally heterogeneous systems. *To be submitted* (2022).

[29] Tzou, J. C., Ward, M. J. & Kolokolnikov, T. Slowly varying control parameters, delayed bifurcations, and the stability of spikes in reaction-diffusion systems. *Physica D: Nonlinear Phenomena* (2015).

[30] Stabb, E. V. The Vibrio fischeri - Euprymna scolopes Light Organ Symbiosis. In *The Biology of Vibrios*, 204–218 (ASM Press, Washington, DC, USA, 2014).

[31] Visick, K. L., Stabb, E. V. & Ruby, E. G. A lasting symbiosis: how Vibrio fischeri finds a squid partner and persists within its natural host. *Nature Reviews Microbiology* **19**, 654–665 (2021).

[32] Pérez, P. D., Weiss, J. T. & Hagen, S. J. Noise and crosstalk in two quorum-sensing inputs of Vibrio fischeri. *BMC Systems Biology* **5**, 153 (2011).

[33] Wu, F., Menn, D. J. & Wang, X. Quorum-Sensing Crosstalk-Driven Synthetic Circuits: From Unimodality to Trimodality. *Chemistry & Biology* **21**, 1629–1638 (2014).

[34] Abreu, C. I., Andersen Woltz, V. L., Friedman, J. & Gore, J. Microbial communities display alternative stable states in a fluctuating environment. *PLoS Computational Biology* **16**, 1–17 (2020).

[35] Mancuso, C. P., Lee, H., Abreu, C. I., Gore, J. & Khalil, A. S. Environmental fluctuations reshape an unexpected diversity-disturbance relationship in a microbial community. *eLife* **10**, 1–31 (2021).

[36] Piñero, J., Redner, S. & Solé, R. Fixation and fluctuations in two-species cooperation. *Journal of Physics: Complexity* **3**, 015011 (2022).

[37] Charlton, T. S. *et al.* A novel and sensitive method for the quantification of N-3-oxoacyl homoserine lactones using gas chromatography-mass spectrometry: Application to a model bacterial biofilm. *Environmental Microbiology* **2**, 530–541 (2000).

[38] Page, K., Maini, P. K. & Monk, N. A. Pattern formation in spatially heterogeneous Turing reaction-diffusion models. *Physica D: Nonlinear Phenomena* **181**, 80–101 (2003).

[39] Page, K. M., Maini, P. K. & Monk, N. A. Complex pattern formation in reaction–diffusion systems with spatially varying parameters. *Physica D: Nonlinear Phenomena* **202**, 95–115 (2005).

[40] Cuesta, C. M. & King, J. R. Front propagation in a heterogeneous fisher equation: The homogeneous case is non-generic. *Quarterly Journal of Mechanics and Applied Mathematics* **63**, 521–571 (2010).

[41] Woolley, T. E., Krause, A. L. & Gaffney, E. A. Bespoke Turing Systems. *Bulletin of Mathematical Biology* **83**, 41 (2021).

[42] Goh, R. & Scheel, A. Pattern-forming fronts in a Swift–Hohenberg equation with directional quenching — parallel and oblique stripes. *Journal of the London Mathematical Society* **98**, 104–128 (2018).

[43] Rüdiger, S., Nicola, E. M., Casademunt, J. & Kramer, L. Theory of pattern forming systems under traveling-wave forcing. *Physics Reports* **447**, 73–111 (2007).

[44] Liu, Y., Maini, P. K. & Baker, R. E. Control of diffusion-driven pattern formation behind a wave of competency. *arXiv* (2021).

[45] Würthner, L. *et al.* Bridging scales in a multiscale pattern-forming system. *arXiv* (2021).

[46] Gomez, M., Moulton, D. E. & Vella, D. Critical slowing down in purely elastic 'snap-through' instabilities. *Nature Physics* **13**, 142–145 (2017).

[47] Liu, M., Gomez, M. & Vella, D. Delayed bifurcation in elastic snap-through instabilities. *Journal of the Mechanics and Physics of Solids* **151**, 104386 (2021).

[48] Singh, P. K. *et al.* Vibrio cholerae Combines Individual and Collective Sensing to Trigger Biofilm Dispersal. *Current Biology* **27**, 3359–3366 (2017).

[49] Coomer, M. A., Ham, L. & Stumpf, M. P. Noise distorts the epigenetic landscape and shapes cell-fate decisions. *Cell Systems* **13**, 83–102 (2021).

[50] Karig, D. *et al.* Stochastic Turing patterns in a synthetic bacterial population. *Proceedings of the National Academy of Sciences* **115**, 6572–6577 (2018).

[51] Michailidi, M. R. *et al.* Morphogen gradient scaling by recycling of intracellular Dpp. *Nature* (2021).

[52] Corson, F. & Siggia, E. D. Geometry, epistasis, and developmental patterning. *Proceedings of the National Academy of Sciences* **109**, 5568–5575 (2012).

[53] Rand, D. A., Raju, A., Sáez, M., Corson, F. & Siggia, E. D. Geometry of gene regulatory dynamics. *Proceedings of the National Academy of Sciences* **118**, e2109729118 (2021).

[54] Sáez, M. *et al.* Statistically derived geometrical landscapes capture principles of decision-making dynamics during cell fate transitions. *Cell Systems* 1–17 (2021).

[55] di Pietro, F. *et al.* Rapid and robust optogenetic control of gene expression in Drosophila. *Developmental Cell* **56**, 3393–3404 (2021).

[56] Hofer, M. & Lutolf, M. P. Engineering organoids. *Nature Reviews Materials* **6**, 402–420 (2021).